Voxel-Based Analysis of Asymmetry Index Maps Increases the Specificity of ^{18}F-MPPF PET Abnormalities for Localizing the Epileptogenic Zone in Temporal Lobe Epilepsies

Adrien Didelot[1–4], François Mauguière[1–5], Jérôme Redouté[6], Sandrine Bouvard[2,6,7], Amélie Lothe[6,7], Anthonin Reilhac[6], Alexander Hammers[5], Nicolas Costes[6], and Philippe Ryvlin[2–4,7,8]

[1]INSERM, U879, Hôpital Pierre Wertheimer, Lyon, France; [2]Université Lyon 1, Lyon, France; [3]Service de Neurologie Fonctionnelle et d'Epileptologie, Hospices Civils de Lyon, Lyon, France; [4]Institut Fédératif des Neurosciences de Lyon, Lyon, France; [5]Neurodis Foundation, Lyon, France; [6]CERMEP—Imagerie du Vivant, Lyon, France; [7]CTRS-INSERM IDEE, Lyon, France; and [8]INSERM, U821, Lyon, France

^{18}F-4-(2′-methoxyphenyl)-1-[2′-(N-2-pyridinyl)-p-fluorobenzamido]-ethyl-piperazine (^{18}F-MPPF) PET has proved to be a sensitive technique in the presurgical evaluation of patients with drug-resistant temporal lobe epilepsy (TLE), but a significant proportion of visually detected abnormalities failed to be detected by standard statistical parametric mapping (SPM) analysis. This study aimed at describing a voxel-based method for computing interhemispheric asymmetric index (AI) using statistical software and applying and validating the clinical relevance of this method for analyzing asymmetries of ^{18}F-MPPF PET images in patients with drug-resistant TLE. **Methods:** ^{18}F-MPPF PET scans of 24 TLE patients who achieved an Engel class I outcome after epilepsy surgery and of 41 controls were analyzed visually, with standard SPM, and by computing voxel-based AIs. Both SPM methods were assessed using 2 different statistical thresholds ($P < 0.05$, corrected at the cluster level, and $P < 0.05$, familywise error (FWE) corrected at the voxel level). Sensitivity and specificity of each method were estimated and compared using McNemar tests. **Results:** The sensitivity of AI analysis to detect decreases of ^{18}F-MPPF binding potential ipsilateral to the epileptogenic lobe was 92% ($P < 0.05$, corrected at the cluster level) and 96% ($P < 0.05$, familywise error corrected at the voxel level), whereas specificity (defined as the congruence between the localization of the voxel associated with the greatest z score and that of the epileptogenic zone) was 88% at both thresholds. AI analysis was significantly more sensitive ($P < 0.05$) and specific ($P < 0.005$) than standard SPM analysis, regardless of the applied threshold. AI analysis also proved to be more sensitive than visual analysis. **Conclusion:** AI analysis of ^{18}F-MPPF PET was more sensitive and specific than previous methods of analysis. This noninvasive imaging procedure was especially informative for the presurgical assessment of patients presenting with clinical histories atypical of mesial TLE or with normal brain MRI results.

Surgical treatment of patients with temporal lobe epilepsy (TLE) leads to seizure freedom in about 2 of 3 patients when the epileptogenic zone (EZ)—defined as the brain region for which resection is both necessary and sufficient to result in seizure freedom [1]—has been removed. There is a need to develop new preoperative investigations to better delineate the EZ in patients in whom temporal lobe surgery has failed. Recent studies suggest that PET tracers targeting the 5-hydroxytryptamine 1A receptor—such as ^{11}C-WAY-100635, ^{18}F-FC-WAY, and ^{18}F-4-(2′-methoxyphenyl)-1-[2′-(N-2-pyridinyl)-p-fluorobenzamido]-ethyl-piperazine (^{18}F-MPPF)—might offer greater sensitivity and specificity than ^{18}F-FDG PET in the delineation of the EZ in TLE patients [2–6]. Voxel-based statistical parametric mapping (SPM) might further improve the diagnostic yield of such PET investigations but was actually found to be less sensitive than visual detection when applied to ^{18}F-MPPF data [6]. We hypothesized that this lesser sensitivity primarily resulted from the wide range of normal binding potential (BP$_{ND}$) values measured within each voxel across healthy subjects [7]. To address this issue, we have developed an SPM-based voxel-by-voxel procedure to calculate and analyze maps of asymmetry index (AI) rather than maps of BP$_{ND}$ values directly, and we evaluated its clinical relevance in 24 patients with drug-resistant TLE, whose EZ localization was validated by a seizure-free outcome after temporal lobectomy.

MATERIALS AND METHODS

Patients and Controls

The 24 patients included in this study fulfilled the following criteria: presurgical evaluation including video electroencephalograph recordings of seizures, brain MRI, and interictal ^{18}F-FDG

PET leading to the diagnosis of unilateral TLE; interictal ^{18}F-MPPF PET; and seizure-free outcome after TLE surgery, defined as an Engel class I (free of disabling seizures) with a postoperative follow-up of at least 8 mo (mean ± SD, 34 ± 12 mo; range, 8 to 53 mo). The BP_{ND} images from this research study were not available at the time of the surgical decision making and were hence not considered for this decision. All these patients belonged to the series of TLE patients previously reported (6), and the clinical features are reported in Supplemental Table 1 (supplemental materials are available online only at http://jnm.snmjournals.org).

The EZ was considered mesial temporal (MT) in 20 patients who benefited from a standard anterior temporal resection (8,9). Of these 20 patients, 13 had the typical electroclinical and MRI features of mesial TLE syndrome, including hippocampal atrophy (8,10); 2 with hippocampal atrophy demonstrated atypical electroclinical findings; and 5 had normal MRI findings. These latter 7 patients underwent invasive-depth stereotactic electroencephalograph examinations, which demonstrated an MT ictal onset in all cases. These 20 patients were classified into subgroups depending on the presence (MT_{HS}) or absence (MT_{noHS}) of hippocampal atrophy on MRI. In the 4 patients not included in the mesial TLE group, ictal onset was localized by electroencephalograph in the lateral temporal (LT) neocortex (NC). The surgical resection was limited to the NC in 2 patients but also involved the MT structures in the 2 others, in whom the ictal discharge rapidly invaded the parahippocampal gyrus and hippocampus (11). These patients were subsequently classified as NC_{MT} or NC_{noMT} according to whether there was early involvement of the MT structures by the ictal discharge. Three of them had normal MRI findings, and 1 had a small lesion located in the middle temporal gyrus that proved to be a focal dysplasia on histopathologic examination.

Regarding the reference database, we used the ^{18}F-MPPF PET images previously obtained in 41 healthy drug-free volunteers without any past history of psychiatric or neurologic illness (mean age, 42.8 y; range, 20–70 y; 23 women) (7), whose brain MRI results were normal plane.

MRI

Structural brain MRI was performed using a 1.5-T Magnetom scanner (Siemens AG) and included a 3-dimensional anatomic T1-weighted sequence covering the whole brain volume, with 1 mm³ cubic voxels; a turbo spin-echo T2-weighted sequence with 6-mm-thick slices acquired parallel to the long axis of the hippocampi; and a turbo spin-echo T2 sequence yielding 3-mm-thick slices perpendicular to the former plane.

^{18}F-MPPF PET

Data Acquisition. ^{18}F-MPPF PET was obtained by nucleophilic fluoration of a nitro precursor with a radiochemical yield of 20%–25% at the end of the synthesis and a specific activity of 32–76 GBq/mmol (12). PET scans were obtained on an HR+ scanner (CTI-Siemens) during the afternoon, after a standard meal. For tracer injections, an intravenous catheter was placed in a vein of the left forearm.

Before emission acquisition, a 10-min transmission scan was acquired using three [68]Ge rod sources for the measurement of tissue and head support attenuation. After intravenous injection of a bolus of ^{18}F-MPPF at 2.7 MBq/kg (mean injected dose, 192 MBq for controls and 184 MBq for patients), a dynamic emission scan consisting of 35 frames of increasing duration (20 s

to 5 min) was acquired during the 60 min after injection. The PET scanner operated in 3-dimensional mode. Images were corrected for scatter and attenuation and reconstructed using filtered backprojection (Hanning filter, cutoff of 0.5 cycles/pixel) to provide a 3-dimensional volume of 63 slices (2.42-mm thickness) with 128 × 128 voxels in-plane (2.06 mm²). The resolution for the reconstructed images was about 6.6 mm in full width at half maximum in the axial direction and 7.1 mm in full width at half maximum in the transaxial direction for a source located at 5 cm from the field of view (13).

Modeling of ^{18}F-MPPF and Creation of Parametric Images of BP_{ND}. For each subject, the MR image was coregistered with mutual information criteria to the static, weighted, and summed PET image to obtain a complete dataset with common orientation and size. Parametric images of BP_{ND} (14) were obtained using an analytic solution for the compartment model, with a simplified reference tissue model validated for ^{18}F-MPPF studies (15). In this model, the assessment of free and nonspecific ligand kinetics is based on the time–activity curve of a reference region (i.e., cerebellar white matter that is devoid of specific 5-hydroxytryptamine 1A receptor binding).

Data Preprocessing. All preprocessing steps were performed using SPM5 software (Wellcome Trust Centre for Neuroimaging; http://www.fil.ion.ucl.ac.uk/spm/software/spm5/). As detailed in the following sections, a different spatial normalization was performed for each method of analysis (standard and AI), using dedicated templates. The reference method of voxel-based analysis was thus used for comparison with the AI analysis.

Preprocessing for SPM Standard Analysis. Raw BP_{ND} images were spatially normalized to a BP_{ND} template in standard MNI/ICBM152 stereotactic space. Normalization parameters were determined from the mean image of the ^{18}F-MPPF dynamic acquisition including all frames from 0 to 60 min and then applied to the raw BP_{ND} images. Normalized images were then smoothed using an isotropic gaussian kernel of 8 mm in full width at half maximum.

Preprocessing for SPM AI Analysis: Symmetric ^{18}F-MPPF PET Template and AI Map Construction (Fig. 1). We first constructed a symmetric ^{18}F-MPPF PET template in approximate standard MNI/ICBM152 stereotactic space using the following procedure, starting from our in-house ^{18}F-MPPF template (T), which—because it was constructed in MNI/ICBM152 space—was naturally nonsymmetric.

1. Flip the initial T around the *x*-axis to create fxT.
2. Add T and fxT to create symT (symmetric, but not exactly centered on the *x* = 0 axis because the flipped and unflipped images showed a small *x* translation (inferior to 1 mm) due to the resolution of PET to MR image registration.
3. Coregister T and fxT on symT independently.
4. Compute the mean of T and fxT, applying the coregistration matrix found in step 3, creating cT (centered, but not necessarily symmetric).
5. Flip cT, creating fxcT.
6. Compute the mean of cT and fxcT. This image is centered and symmetric and corresponds to our "symmetric ^{18}F-MPPF template" in the subsequent procedure.

For AI map construction, raw (unnormalized) BP_{ND} images of patients and controls were spatially normalized to this symmetric template using SPM5. Normalized BP_{ND} images were spatially
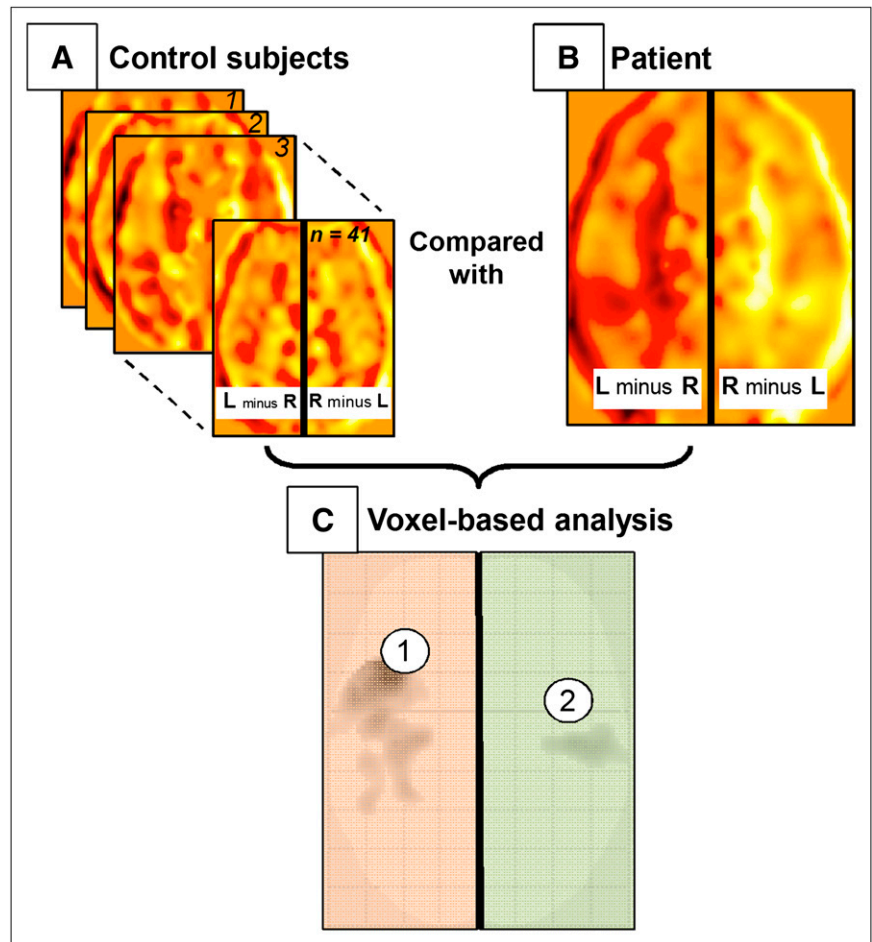
FIGURE 1. AI analysis. (A) Maps of AIs obtained from control BP_{ND} datasets. (B) Map of AIs obtained from BP_{ND} images of patient under study. (C) Maximum-intensity projection viewed from above represents AI map. Orange area corresponds to the contrast "left hemisphere minus right hemisphere" and green area to "right hemisphere minus left hemisphere." Resulting voxel-based statistical analysis was performed using SPM5 at $P < 0.05$ corrected at cluster level. In this example, 2 clusters were identified by AI analysis: one (in orange part of maximum-intensity projection): $(R - L)_{Patient} > (R - L)_{Controls}$, consistent with left decrease or right increase of MPPF BP_{ND} in patient, and the second (in green part of maximum-intensity projection): $(L - R)_{Patient} > (L - R)_{Controls}$, consistent with right decrease or left increase of MPPF BP_{ND} in patient.

smoothed using an 8-mm isotropic gaussian kernel to correct for remaining intersubject anatomy variability. Areas with BP_{ND} less than 0.05 were excluded by thresholding to remove low values. The resulting thresholded and smoothed normalized image (V_{BP}) was right–left reversed, providing its flipped BP_{ND} counterpart (fV_{BP}). An AI volume (V_{AI}) was then computed using the Volumes Toolbox (http://sourceforge.net/projects/spmtools) of the SPM software package, according to the following formula:

$$V_{AI} = (V_{BP} - fV_{BP})/(V_{BP} + fV_{BP}),$$

so that at each voxel, the resulting value represented the AI calculated at that position. Finally, we applied a second spatial smoothing using an isotropic 4-mm gaussian kernel to correct for the small bias that could be induced by the flipping step. This second spatial smoothing step resulted in a final smoothness of the SPM AI analysis of about 10–15 mm, similar to that of standard analysis.

Statistical Analysis of BP_{ND} and AI Images

Statistical Design for BP_{ND} and AI Analysis. BP_{ND} and AI images from patients were individually compared with controls' BP_{ND} and AI images, respectively, using the 2-sample t test of the SPM software package, with an ANCOVA by subject, equal variance, and without overall grand mean scaling. Analysis was restricted to voxels belonging to gray matter by applying a mask obtained by thresholding at $x > 0.3$ the probabilistic map of gray matter within the SPM distribution (/spm5/apriori/gray.nii). A symmetric mask, obtained using the same procedure as for the symmetric template, was used for AI analysis. Age and sex were modeled as covariates of no interest (*15*). Two different thresholds were chosen considering the results of another study (*16*) and were applied for each analysis: $P < 0.05$, familywise error (FWE) corrected at the voxel level, representing a stringent statistical criterion for this type of analysis, and $P < 0.05$, corrected at the cluster level (clusters are defined by voxels surviving a threshold of $P < 0.001$ uncorrected).

Direction of BP_{ND} Abnormalities Underlying AI Increases. Because many ^{18}F-MPPF PET abnormalities in patients with TLE correspond to decreases of BP_{ND}, we selected the contrast Controls – Patients, which displayed a significant AI resulting from decreased BP_{ND} on the same side as the underlying standard BP_{ND} abnormality. For example, the left half of the map corresponds to the following algebraic calculation: (right hemisphere – left hemisphere)$_{patient}$ – (right hemisphere – left hemisphere)$_{controls}$; thus, any significant cluster reflects either a left-sided BP_{ND} decrease or a less likely right-sided BP_{ND} increase in the patient, as compared with controls (Fig. 2). To further ensure the direction of BP_{ND} changes underlying AI abnormalities, we used the results provided in the same brain regions by standard SPM analysis. When the latter were negative at the threshold considered for statistical significance (see the previous paragraph), we searched
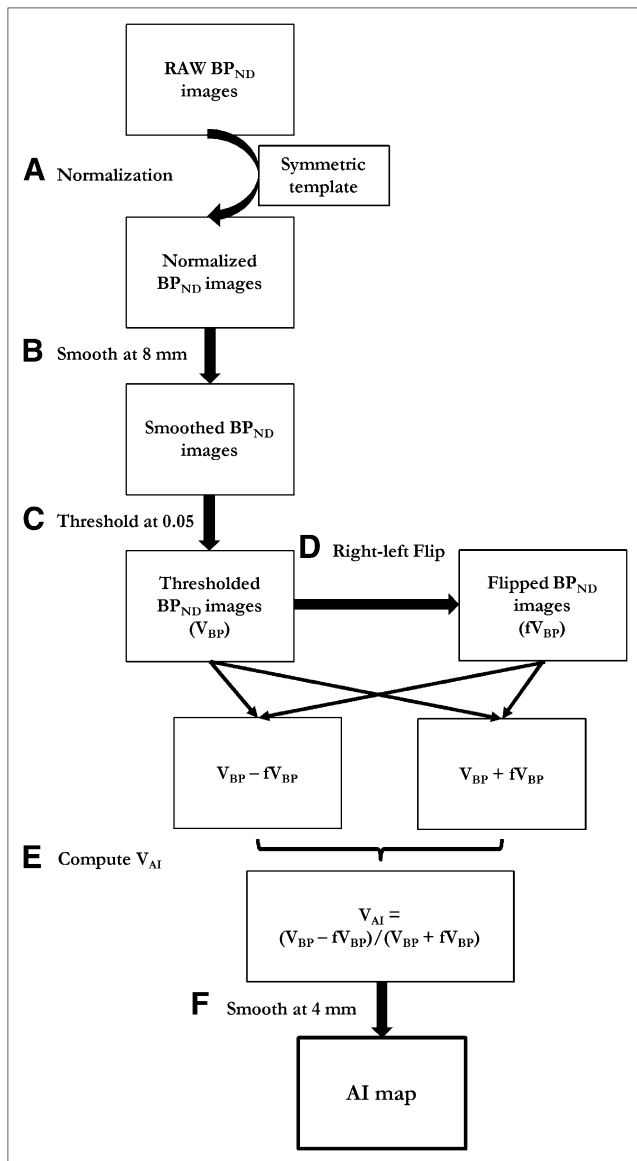
FIGURE 2. Flowchart showing construction of AI maps. Raw BP_{ND} images correspond to unnormalized BP_{ND} images that have not been spatially normalized.

for clusters at $p_{uncorrected} < 0.005$ and, if still negative, at $p_{uncorrected} < 0.01$. This procedure allowed us to determine the type of abnormality underlying significant AIs in all cases.

Interpretation of BP_{ND} Parametric Images and Statistical Parametric Maps

The location of the maximal ^{18}F-MPPF BP_{ND} abnormality could not be reliably assessed by visual analysis according to the consensual opinion of the 3 PET experts who reviewed the entire dataset. Consequently, we have limited our clinical analysis to data showing a BP_{ND} decrease after either visual, standard SPM, or AI analyses. Two criteria were considered—first, the presence and location of clusters showing significant abnormalities, and second, the location of the maximal abnormality defined as the voxel from any significantly abnormal cluster that showed the highest z score (z max). We chose to consider 3 anatomic regions based on the EZ location to

compare our different methods of analysis (visual, standard SPM, and AI). The MT region included the amygdala, hippocampus, parahippocampal gyrus, and mesial aspect of the temporal pole. The lateral temporal (LT) region included the superior, middle, and inferior temporal gyri and lateral occipitotemporal (fusiform) gyrus and the lateral aspect of the temporal pole. The third region included all extratemporal (ET) cortical regions.

The visual analysis of BP_{ND} parametric images has been described in our previous study (6). Briefly, all TLE scans intermixed with control scans from healthy subjects matched for age and sex were visually and separately analyzed by 3 experts unaware of the patients' clinical histories and other presurgical data. Experts were asked to report on the presence and location of visible areas of BP_{ND} decrease but not on the location of the site with maximal abnormality because the latter could not be assessed visually in a reliable manner.

Statistical parametric maps were superimposed on MR images to precisely assess the anatomic location of all significant clusters and that of the voxel with the highest z score and to ascribe these abnormalities to 1 of the 3 anatomic regions (MT, LT, or ET).

Sensitivity and Specificity

Sensitivity and specificity of each method of analysis were defined as follows. Sensitivity was the proportion of all ^{18}F-MPPF PET images showing the decrease of BP_{ND} to encompass the EZ as defined for each patient. Specificity corresponded to the proportion of all ^{18}F-MPPF PET images showing the maximum BP_{ND} decrease to be within the EZ. Sensitivity and specificity of all methods of analysis were compared using the McNemar test.

RESULTS

Visual Analysis

As described in detail in our previous study (6), investigators agreed on the presence of a focally decreased BP_{ND} in 20 of 24 patients (83%), including 100% of the 15 patients with MT_{HS}, but only 3 (60%) of the 5 MT_{noHS} patients, and 50% of the other patients (1 NC_{MT} and 1 NC_{noMT} patient). These abnormalities primarily involved the epileptogenic temporal lobe in all cases but extended to the temporal NC or ET regions in 14 (70%) of the 20 MT patients, to the ET region in 1 of the 2 NC_{MT} patients, and to the MT region in 1 of the 2 NC_{noMT} patients.

Standard SPM Analysis

P < 0.05 Threshold FWE-Corrected at Voxel Level (Fig. 3). At least 1 significant cluster of decreased BP_{ND} was observed in 14 patients (58%) overall, 9 of 15 (60%) MT_{HS} patients, 3 of 5 (60%) MT_{noHS} patients, 1 of 2 (50%) NC_{noMT} patients, and none of the 2 NC_{MT} patients. These abnormalities were ipsilateral to the EZ in all patients and involved the epileptogenic temporal lobe in 12 of 24 patients—that is, the overall sensitivity was 50%. In 1 MT_{HS} and 1 NC patient, the only significant cluster was ET. The voxel with the highest z score was located in the MT structures and hence correctly identified the EZ in 7 MT_{HS} patients and 1 MT_{noHS} patient, whereas it was located in the LT cortex in 2 MT_{noHS} patients and 1 MT_{HS} patient and in ET regions in 1 MT_{HS} patient. In the 2 NC patients with significant clusters) of decreased BP_{ND}, the

Figure 3

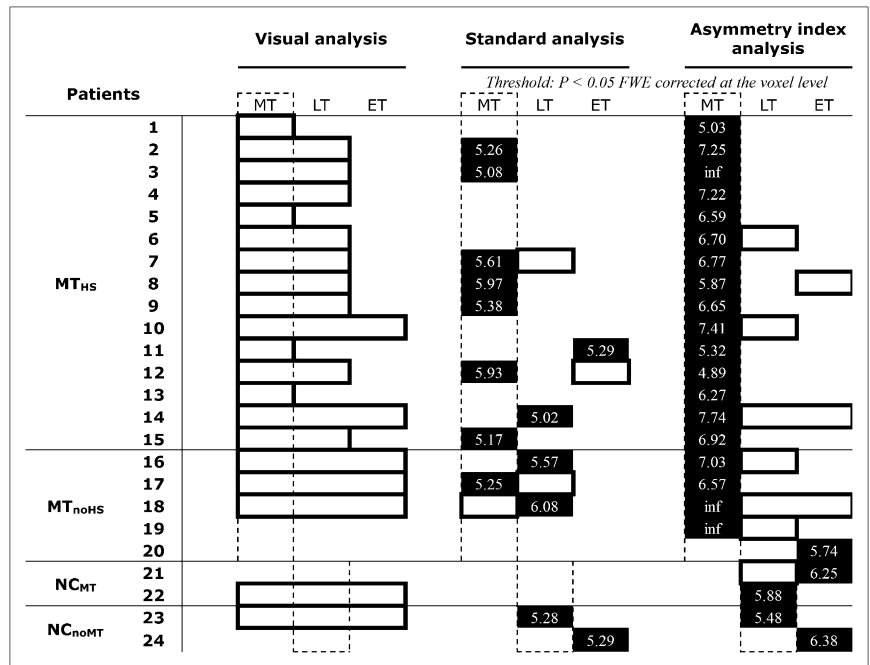|	Patients	Visual analysis MT	LT	ET	Standard analysis MT	LT	ET	Asymmetry index analysis MT	LT	ET
					Threshold: P < 0.05 FWE corrected at the voxel level					
MT$_{HS}$	1							5.03		
	2				5.26			7.25		
	3				5.08			inf		
	4							7.22		
	5							6.59		
	6							6.70		
	7				5.61			6.77		
	8				5.97			5.87		
	9				5.38			6.65		
	10							7.41		
	11						5.29	5.32		
	12				5.93			4.89		
	13							6.27		
	14					5.02		7.74		
	15				5.17			6.92		
MT$_{noHS}$	16					5.57		7.03		
	17				5.25			6.57		
	18					6.08		inf		
	19							inf		
	20									5.74
NC$_{MT}$	21									6.25
	22								5.88	
NC$_{noMT}$	23					5.28			5.48	
	24						5.29			6.38

FIGURE 3. Results of visual, standard, and AI analyses. Statistical threshold: $P < 0.05$, FWE-corrected at voxel level. Dotted line delineates suspected EZ for each TLE subgroup: MT and LT for MT and NC patients, respectively. Significant BP$_{ND}$ decreases are reported for each region of interest by squared boxes. Black boxes represent region in which voxel associated with maximal z score is located.

voxel with the highest z score was located in the LT cortex in one patient and in an ET region in the other. According to our definition, the specificity of this standard SPM analysis was 64% (representing 9/14 patients in whom significant ^{18}F-MPPF PET abnormalities were found and in whom the voxel with the highest z score was located in the EZ).

P < 0.05 Threshold Corrected at Cluster Level (Fig. 4). At this more liberal threshold, 5 additional patients had significant clusters of decreased BP$_{ND}$. These were located in the epileptogenic temporal lobe in 4 and in ipsilateral ET regions in 1. Overall, sensitivity increased from 50% to 67% (i.e., 16/24 patients had a cluster of significantly decreased BP$_{ND}$ in the epileptogenic temporal lobe). Conversely, specificity decreased from 64% to 47%, with the voxel associated with highest z score being located within the EZ in only 9 of the 19 patients with significant clusters of decreased BP$_{ND}$ (7 MT$_{HS}$ patients, 1 MT$_{noHS}$ patient, and 1 NC patient). Six MT$_{HS}$ and 3 MT$_{noHS}$ patients had the highest z score voxel located either in the LT cortex ($n = 7$) or in the ET regions ($n = 2$). Furthermore, 2 patients (1 NC$_{MT}$ and 1 NC$_{noMT}$) had their maximum abnormality located in ET regions.

Figure 4

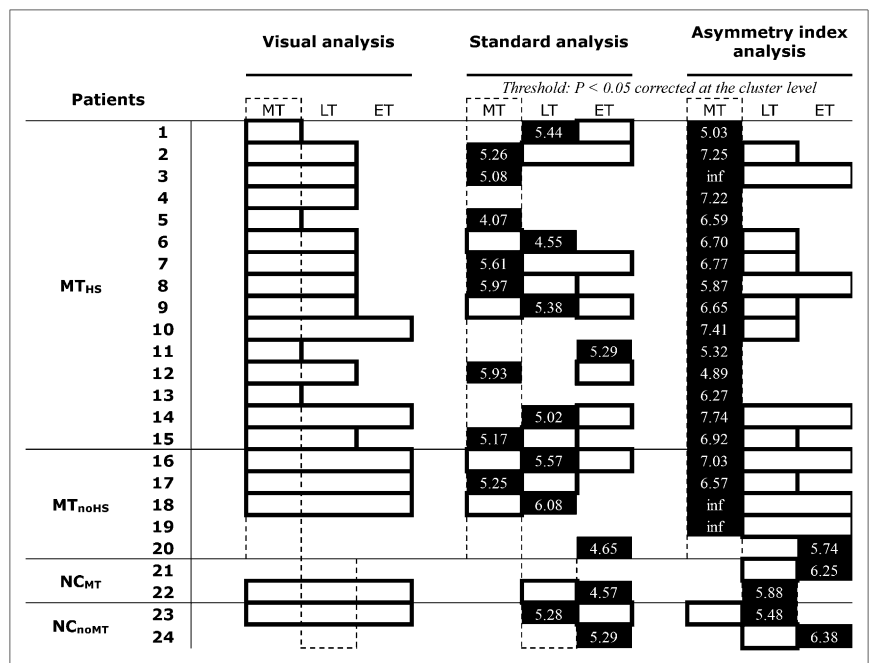|	Patients	Visual analysis MT	LT	ET	Standard analysis MT	LT	ET	Asymmetry index analysis MT	LT	ET
					Threshold: P < 0.05 corrected at the cluster level					
MT$_{HS}$	1					5.44		5.03		
	2				5.26			7.25		
	3				5.08			inf		
	4							7.22		
	5				4.07			6.59		
	6					4.55		6.70		
	7				5.61			6.77		
	8				5.97			5.87		
	9					5.38		6.65		
	10							7.41		
	11						5.29	5.32		
	12				5.93			4.89		
	13							6.27		
	14					5.02		7.74		
	15				5.17			6.92		
MT$_{noHS}$	16					5.57		7.03		
	17				5.25			6.57		
	18					6.08		inf		
	19							inf		
	20						4.65			5.74
NC$_{MT}$	21									6.25
	22					4.57			5.88	
NC$_{noMT}$	23					5.28			5.48	
	24						5.29			6.38

FIGURE 4. Results of visual, standard, and AI analysis. Statistical threshold: $P < 0.05$, corrected at cluster level. Dotted line delineates suspected EZ for each TLE subgroup: MT and LT for MT and NC patients, respectively. Significant BP$_{ND}$ decreases are reported for each region of interest by squared boxes. Black boxes represent region in which voxel associated with maximal z score is located.

AI Analysis

P < 0.05 Threshold FWE-Corrected at Voxel Level (Fig. 3). A significant abnormality was observed in all patients at this threshold. In each patient, the comparison of the result with the standard SPM analysis demonstrated that the main AI clusters always corresponded to a decreased BP_{ND} ipsilateral to the epileptogenic temporal lobe. In all but 2 patients (patients 20 and 24), the significant AI clusters involved the temporal lobe, yielding a sensitivity of 92% (22/24 patients) (15/15 [100%] for MT_{HS}, 4/5 [80%] for MT_{noHS}, 2/2 [100%] for NC_{MT}, and 1/2 [50%] for NC_{noMT} patients). The voxel with the highest z score was located within the EZ in 21 of 24 patients, including all 15 MT_{HS} patients, 4 of 5 (80%) MT_{noHS} patients, and 2 of 4 (50%) NC patients. Thus, the specificity was 88% (21/24) according to our definition.

P < 0.05 Threshold Corrected at Cluster Level (Fig. 4). At this more liberal threshold, 1 additional NC patient had a significant cluster in the epileptogenic temporal lobe, increasing sensitivity from 92% to 96%, whereas specificity remained at 88%.

Comparing Visual, Standard, and AI SPM Analyses

AI analysis was more sensitive than standard analysis for both statistical SPM thresholds ($P < 0.001$ and $P < 0.05$ for the most and least stringent SPM thresholds, respectively). Similarly, AI analysis was more specific than standard analysis ($P < 0.005$ for both statistical thresholds). Neither SPM nor AI analysis proved significantly more sensitive than visual analysis, even though they detected abnormalities in the 4 patients in whom visual analysis proved normal. Standard SPM analysis disclosed significant clusters in 2 of these 4 patients, but these clusters were restricted to ET regions and thus considered irrelevant. In contrast, AI analysis detected a significant cluster within the epileptogenic temporal lobe in 3 of the 4 patients, compared with normal visual analysis (Fig. 5; Supplemental Fig. 1). Furthermore, in patients in whom visual inspection of ^{18}F-MPPF PET detected an abnormality, the localization of the z max score derived from AI analysis provided reliable information regarding the sublobar origin of the seizure onset, which could not be obtained by visual analysis.

DISCUSSION

In this study we have developed a voxel-based statistical analysis of the interhemispheric AI of ^{18}F-MPPF PET images and validated this method in the context of presurgical evaluation of TLE patients. This approach proved highly sensitive for identifying focal BP_{ND} decreases that correctly identified side, lobar, and sublobar localization of the EZ in most patients.

Advantages of Voxel-Based AI Analysis

Regarding the lateralization of the epileptogenic temporal lobe, voxel-based AI analysis proved significantly more sensitive than standard SPM analysis, with a detection rate of 100% versus 58% at a statistical threshold of $P < 0.05$ FWE. The reason for this difference is likely to reflect the larger variation of BP_{ND} values, as compared with BP_{ND} ratio at the voxel level across controls. Indeed, AIs allow within-subject normalization that has been found to be beneficial in other contexts, too (*17*). Furthermore, AI analysis detected significant abnormalities, half of which were colocalized with the EZ, in all 4 patients in whom visual analysis was negative.

Several other computerized techniques based on region-of-interest measurements have consistently demonstrated the effectiveness of AI analysis for lateralizing the EZ, using either
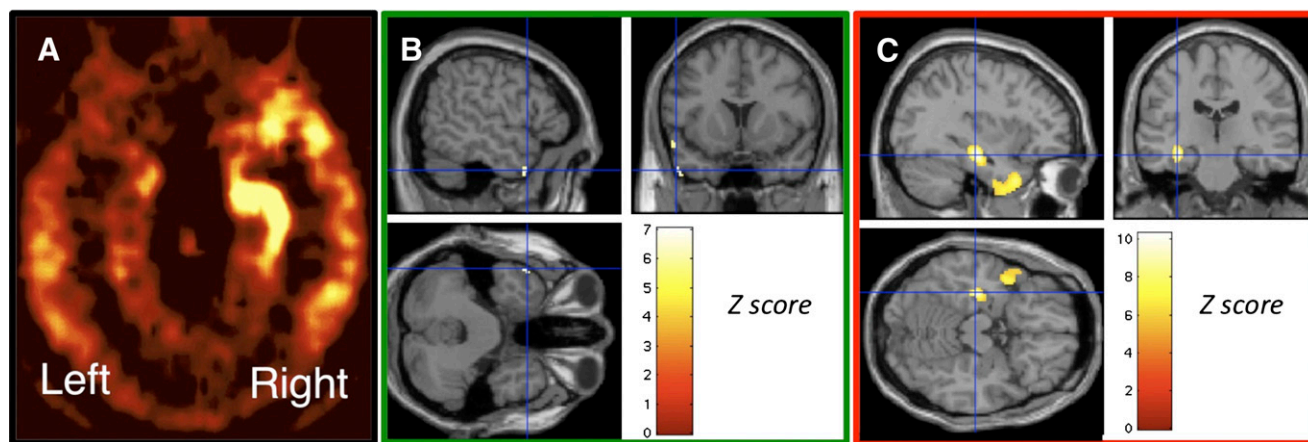

FIGURE 5. Results of visual, standard, and AI analysis of patient with MT lobe epilepsy (MT_{noHS}, patient 16). (A) Axial slice of BP_{ND} map in plane along long axis of hippocampi showing visually detectable left-sided decreased ^{18}F-MPPF binding involving entire temporal lobe and extending to ipsilateral ET regions. (B) Standard analysis: projection of significant clusters obtained by SPM5 analysis at statistical level of $P < 0.05$, FWE-corrected at voxel level onto patient's normalized MR image. Blue cross indicates voxel with highest z score located in anterior part of inferior temporal gyrus. (C) AI analysis: projection of significant clusters obtained with SPM5 analysis at statistical threshold of $P < 0.05$, FWE-corrected at voxel level onto patient's normalized MR image. Blue cross indicates voxel with highest z score, located within epileptogenic hippocampus.

^{18}F-FDG PET, α-methyl tryptophan, or radiolabeled ligands of benzodiazepine (^{11}C-flumazenil-PET) or 5-hydroxytryptamine 1A receptors (^{18}F-CWAY PET) *(4,18,19)*. The advantage of voxel-based AI analysis is that, unlike methods based on regions of interest, it does not require any a priori hypothesis on the location or extent of the suspected abnormalities. Van Bogaert et al. *(20)* proposed a similar approach for analyzing AIs of glucose metabolism using ^{18}F-FDG PET in 12 TLE patients. As in our ^{18}F-MPPF PET study, this approach proved more reliable than standard SPM analysis in lateralizing the epileptogenic temporal lobe.

Specificity, defined here as the proportion of patients in whom the voxel showing the highest z score correctly identified the sublobar localization of the EZ, was also greater for AI than for standard SPM analysis. Previous studies of AI have not addressed this issue, which in our view represents one of the major benefits of AI analysis, as compared with visual analysis. Indeed, defining the area of maximal abnormality using visual analysis was extremely difficult and poorly reliable. The great intrahemispheric variability of ^{18}F-MPPF binding between limbic, paralimbic, and neocortical regions hampers any robust visual comparison of the degree of asymmetry across these various brain structures. Interestingly, the only 2 MT patients who were not completely seizure-free (Engel class Ib/Ic) either had an ET maximal AI z score (patient 20) or had a large cluster extending to a large portion of the ipsilateral ET region (patient 13).

Limitations of Voxel-Based AI Analysis

Several technical limitations of our procedure need to be discussed. The generation of artifacts within a limited volume of several tens of voxels was centered over the interhemispheric midline, which may hamper the interpretation of decreased BP_{ND} in mesial frontal, parietal, and occipital cortical areas. These midline artifacts, which were observed in 21% of patients, have no major impact in TLE but limit the application of our method in patients with partial epilepsies with suspected involvement of the mesial ET regions. Further refinements of image coregistration and normalization methods may help to address this issue.

Another limitation of our method is the symmetrization of the physiologically asymmetric brain. The deformation of the brain, resulting from the normalization step to the symmetric template, is different for left and right hemispheres, potentially influencing the yield of AI analysis as a function of the lateralization of the epileptogenic temporal lobe. Our findings did not suggest any such influence, because the same proportion of patients with right or left TLE demonstrated significant AI abnormalities, regardless of their hemispheric dominance.

Our method cannot directly provide information as to whether an abnormal AI primarily reflects increased binding on one side or decreased binding on the other. However, post hoc analysis of standard statistical parametric maps at various statistical thresholds easily allows the determination of which of the 2 above-mentioned hypotheses is cor-

rect. In our populations of TLE patients, abnormal AIs within temporal lobes always reflected BP_{ND} decreases ipsilateral to the EZ. AI increases reflecting increased BP_{ND} were uncommon, observed only in ET regions, and always smaller and less significant than BP_{ND} decreases. The SPM script automatically generates AI and standard statistical parametric maps, allowing an unambiguous and time-efficient detection and interpretation of significant AI abnormality in clinical practice. The script is available from http://www.cermep.fr/download.

Limitations of Study Design

The relatively limited number of patients, especially those with the EZ located in the LT NC (NC group), and the selection of seizure-free postsurgical outcomes (Engel class I patients) that was needed to evaluate the sensitivity and specificity of our procedure is a limitation of our study. Thus, this selection did not allow us to address the issue of whether patients with poor surgery outcome would present with AI patterns similar to, or different from, those observed in Engel class I patients. Similarly we did not explore the value of ^{18}F-MPPF PET and AI analysis in ET lobe epilepsy or temporal plus epilepsy *(21)*.

Clinical Relevance of AI Analysis

From a clinical point of view, ^{18}F-MPPF PET appears useful for TLE patients with normal MRI or normal ^{18}F-FDG PET findings, in whom the risks of a misdiagnosis such as ET lobe epilepsy or temporal lobe surgery failure are minimized. In such patients, ^{18}F-MPPF PET appears likely to detect abnormalities within the epileptogenic temporal lobe. In particular, when MRI findings are normal, ^{18}F-MPPF PET findings might help in decisions whether to perform and tailor an invasive intracranial electroencephalograph investigation. In this context, AI analysis proved more sensitive than all other methods and also helped identify the most likely sublobar localization of the EZ. However, one should keep in mind that, despite the concordance observed between the localization of the EZ and that of the maximal ^{18}F-MPPF AI abnormality, the latter does not precisely map the extent of the EZ.

CONCLUSION

Overall, the combined use of visual and voxel-based AI and standard SPM analysis improves the diagnostic yield of ^{18}F-MPPF PET in patients with TLE who are candidates for epilepsy surgery. This approach deserves to be further developed with other PET tracers, including ^{18}F-FDG PET, and in ET lobe epilepsies. It should also facilitate a more objective comparison of the various imaging techniques used in the presurgical evaluation of refractory partial epilepsies.

ACKNOWLEDGMENTS

REFERENCES

1. Rosenow F, Luders H. Presurgical evaluation of epilepsy. *Brain*. 2001;124:1683–1700.

2. Merlet I, Ryvlin P, Costes N, et al. Statistical parametric mapping of 5-HT1A receptor binding in temporal lobe epilepsy with hippocampal ictal onset on intracranial EEG. *Neuroimage*. 2004;22:886–896.

3. Savic I, Lindstrom P, Gulyas B, Halldin C, Andree B, Farde L. Limbic reductions of 5-HT1A receptor binding in human temporal lobe epilepsy. *Neurology*. 2004;62:1343–1351.

4. Toczek MT, Carson RE, Lang L, et al. PET imaging of 5-HT1A receptor binding in patients with temporal lobe epilepsy. *Neurology*. 2003;60:749–756.

5. Merlet I, Ostrowsky K, Costes N, et al. 5-HT1A receptor binding and intracerebral activity in temporal lobe epilepsy: an [^{18}F]MPPF-PET study. *Brain*. 2004;127:900–913.

6. Didelot A, Ryvlin P, Lothe A, Merlet I, Hammers A, Mauguiere F. PET imaging of brain 5-HT1A receptors in the preoperative evaluation of temporal lobe epilepsy. *Brain*. 2008;131:2751–2764.

7. Costes N, Merlet I, Ostrowsky K, et al. A ^{18}F-MPPF PET normative database of 5-HT1A receptor binding in men and women over aging. *J Nucl Med*. 2005;46:1980–1989.

8. Williamson PD, French JA, Thadani VM, et al. Characteristics of medial temporal lobe epilepsy: II. Interictal and ictal scalp electroencephalography, neuropsychological testing, neuroimaging, surgical results, and pathology. *Ann Neurol*. 1993;34:781–787.

9. Spencer DD, Spencer SS. Surgery for epilepsy. *Neurol Clin*. 1985;3:313–330.

10. French JA, Williamson PD, Thadani VM, et al. Characteristics of medial temporal lobe epilepsy: I. Results of history and physical examination. *Ann Neurol*. 1993;34:774–780.

11. Kahane P, Landre E, Minotti L, Francione S, Ryvlin P. The Bancaud and Talairach view on the epileptogenic zone: a working hypothesis. *Epileptic Disord*. 2006;8(suppl 2):S16–S26.

12. Le Bars D, Lemaire C, Ginovart N, et al. High-yield radiosynthesis and preliminary in vivo evaluation of p-[^{18}F]MPPF, a fluoro analog of WAY-100635. *Nucl Med Biol*. 1998;25:343–350.

13. Frouin V, Comtat C, Reilhac A, Gregoire MC. Correction of partial-volume effect for PET striatal imaging: fast implementation and study of robustness. *J Nucl Med*. 2002;43:1715–1726.

14. Innis RB, Cunningham VJ, Delforge J, et al. Consensus nomenclature for in vivo imaging of reversibly binding radioligands. *J Cereb Blood Flow Metab*. 2007;27:1533–1539.

15. Costes N, Merlet I, Zimmer L, et al. Modeling [18 F]MPPF positron emission tomography kinetics for the determination of 5-hydroxytryptamine$_{1A}$ receptor concentration with multiinjection. *J Cereb Blood Flow Metab*. 2002;22:753–765.

16. Redouté J, Reilhac A, Didelot A, Ryvlin P, Costes N. Voxel based asymmetry index maps analysis: principle and validation with MPPF PET simulated data. Paper presented at: 16th Annual Meeting of the Organization for Human Brain Mapping; June 6–10, 2010; Barcelona, Spain.

17. Hammers A, Asselin MC, Turkheimer FE, et al. Balancing bias, reliability, noise properties and the need for parametric maps in quantitative ligand PET: [^{11}C] diprenorphine test-retest data. *Neuroimage*. 2007;38:82–94.

18. Muzik O, Chugani DC, Shen C, et al. Objective method for localization of cortical asymmetries using positron emission tomography to aid surgical resection of epileptic foci. *Comput Aided Surg*. 1998;3:74–82.

19. Lin TW, de Aburto MA, Dahlbom M, et al. Predicting seizure-free status for temporal lobe epilepsy patients undergoing surgery: prognostic value of quantifying maximal metabolic asymmetry extending over a specified proportion of the temporal lobe. *J Nucl Med*. 2007;48:776–782.

20. Van Bogaert P, Massager N, Tugendhaft P, et al. Statistical parametric mapping of regional glucose metabolism in mesial temporal lobe epilepsy. *Neuroimage*. 2000;12:129–138.

21. Ryvlin P, Kahane P. The hidden causes of surgery-resistant temporal lobe epilepsy: extratemporal or temporal plus? *Curr Opin Neurol*. 2005;18:125–127.